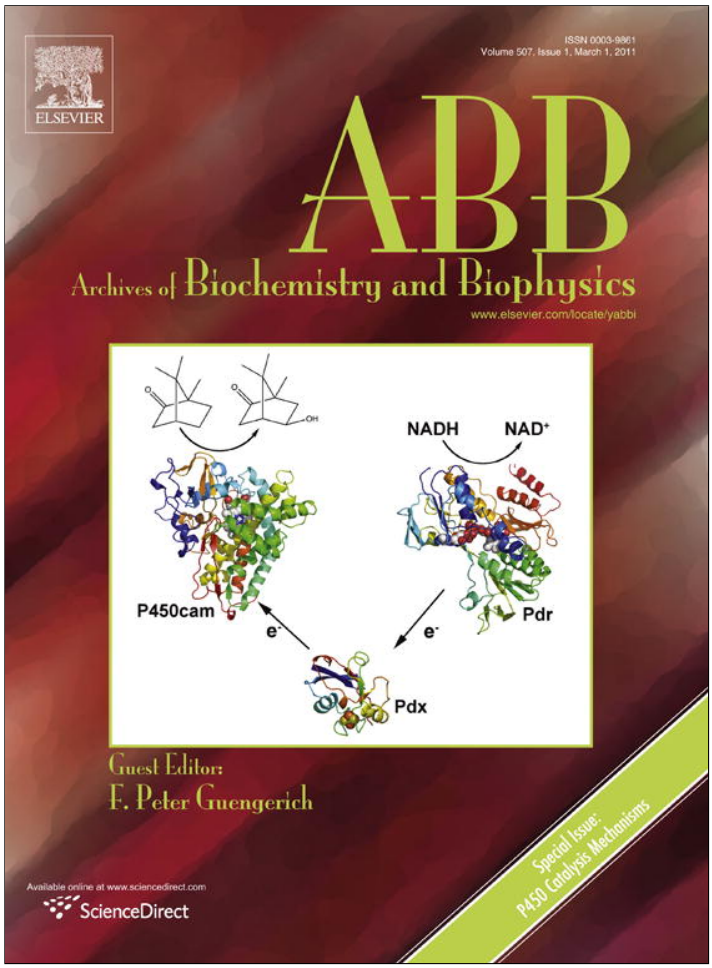

Archives of Biochemistry and Biophysics 507 (2011) 4–13

Contents lists available at ScienceDirect

Archives of Biochemistry and Biophysics

journal homepage: www.elsevier.com/locate/yabbi

Manganese substituted Compound I of cytochrome P450 biomimetics: A comparative reactivity study of Mn^{V}-oxo versus Mn^{IV}-oxo species

Reza Latifi [a,b,c], Laleh Tahsini [a,c], Baharan Karamzadeh [a], Nasser Safari [b], Wonwoo Nam [c,d,*], Sam P. de Visser [a,*]

[a] The Manchester Interdisciplinary Biocenter, School of Chemical Engineering and Analytical Science, The University of Manchester, 131 Princess Street, Manchester M1 7DN, United Kingdom
[b] Chemistry Department, Shahid Beheshti University, Evin, Tehran 1983963113, Iran
[c] Department of Bioinspired Science, Centre for Biomimetic Systems, Ewha Womans University, Seoul 120-750, South Korea
[d] Department of Chemistry and Nano Science, Centre for Biomimetic Systems, Ewha Womans University, Seoul 120-750, South Korea

ARTICLE INFO

Article history:
Available online 7 January 2011

Keywords:
Biomimetic
Porphyrin
Hydroxylation
Hydride transfer
Manganese-oxo
Iron-oxo

ABSTRACT

Manganese-oxo porphyrins have been well studied as biomimetic models of cytochromes P450 and are known to be able to catalyze substrate hydroxylation reactions. Recent experimental studies [J.Y. Lee, Y.-M. Lee, H. Kotani, W. Nam, S. Fukuzumi, Chem. Commun. (2009) 704] showed that Mn(V)-oxo porphyrins react rapidly with 10-methyl-9,10-dihydroacridine ($AcrH_2$) via a proton-coupled-electron-transfer followed by an electron transfer. In this work, we present a computational study on the reactivity patterns of Mn(V)-oxo and Mn(IV)-oxo with respect to $AcrH_2$. This study shows that although both oxidants are capable of hydroxylating $AcrH_2$, the Mn^{V}-oxo species is the more active oxidant. We have generalized these observations with thermodynamic cycles that explain the reaction mechanisms and electron transfer processes. For the Mn^{V}-oxo mechanism the reactions proceed with a fast spin state crossing from the ground state singlet to the triplet spin state prior to a hydrogen atom transfer followed by another electron transfer. The present results are fully consistent with previous studies on iron-oxo porphyrins and manganese-oxo porphyrins and shows that the interplay of low lying singlet and triplet spin state surfaces influences the reaction mechanisms and kinetics.

Introduction

The cytochromes P450 are vital enzymes for human health and are involved in the biodegradation of toxic compounds, including the metabolism of drugs [1–6]. They bind molecular oxygen on a heme center and transfer one of its oxygen atoms to a substrate, while the other oxygen atom originating from O_2 is reduced to a water molecule. The P450s are versatile monoxygenation catalysts that perform substrate hydroxylation (aliphatic and aromatic), epoxidation, heteroatom oxidation and dehydrogenation processes [7,8]. Often these reactions are stereospecific or regioselective and hence there is commercial interest in their utilization for the biosynthesis of drugs and pharmaceuticals. Despite the high interest of scientists in these enzymes, there are still significant gaps in understanding of the mechanism of P450 enzymes, which is partially due to the fact that its active species, termed Compound I (Cpd I)[1], has never been detected. So far, indirect evidence from kinetic isotope effect and product distribution studies implicated an iron(IV)-oxo heme cation radical as the active species [9,10]. This is supported by many biomimetic studies of iron-porphyrins that also implicate an iron(IV)-oxo porphyrin cation radical as the active oxidant [7,8,11–14].

An extract of the catalytic cycle of P450 enzymes is given in Scheme 1. Thus, the reaction starts from the resting state where a water molecule binds to the distal ligand site of the heme, while a thiolate group of a cysteinate residue is bound on the proximal (axial) site. After this water molecule is released upon binding substrate (SubH), the system is reduced by one electron and then binds molecular oxygen prior to a second electron transfer. The iron(III)-peroxo complex is protonated by a proton from a nearby proton source to give the ferric-hydroperoxo complex that is also

* Corresponding authors. Addresses: Department of Bioinspired Science, Department of Chemistry and Nano Science, EWHA Womans University, Seoul 120-750, South Korea (W. Nam), The Manchester Interdisciplinary Biocenter, School of Chemical Engineering and Analytical Science, The University of Manchester, 131 Princess Street, Manchester M1 7DN, United Kingdom (S.P. de Visser).
E-mail addresses: wwnam@ewha.ac.kr (W. Nam), sam.devisser@manchester.ac.uk (S.P. de Visser).

[1] *Abbreviations used:* Cpd I, Compound I; SOD, superoxide dismutase; $AcrH_2$, 10-methyl-9,10-dihydroacridine; DFT, density functional theory; ZPE, zero-point energy; Por, porphyrin; TDCPP, *meso*-tetrakis(2,6-dichlorophenyl)porphyrin.

0003-9861/$ - see front matter © 2011 Elsevier Inc. All rights reserved.
doi:10.1016/j.abb.2010.12.035

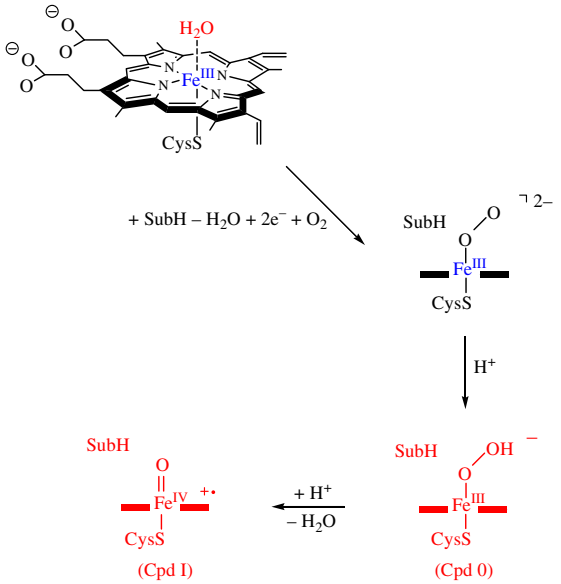

Scheme 1. Extract of the catalytic cycle of P450 enzymes with key intermediates (Cpd I and Cpd 0) highlighted.

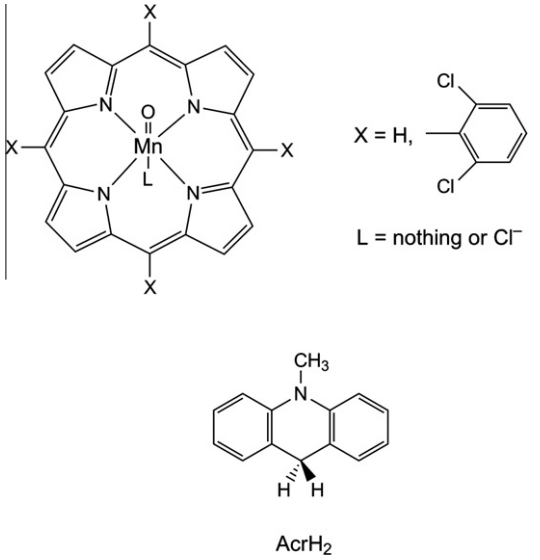

Scheme 2. Manganese(IV and V)-oxo oxidants and substrate ($AcrH_2$) studied in this work.

known as Compound 0 (Cpd 0). A subsequent protonation step then leads to a ferryl heme cation radical complex or Compound I (Cpd I). This is the active species of the enzyme that abstracts a hydrogen atom from the substrate and rebounds the OH group to give an alcohol product.

Some P450 mutants as well as superoxide dismutase (SOD) enzymes utilize manganese rather than iron in their catalytic center [15–17]. As chemical models of Cpd I of P450, the analogous manganese(V)-oxo and their one electron reduced form, manganese(IV)-oxo, have been extensively investigated previously [18]. However, only recently full spectroscopic characterization of these species was achieved through UV–vis, ^{1}H NMR, resonance Raman, and X-ray absorption [19–23]. Since then several reactivity studies of manganese-oxo complexes have been reported [24–45]. In particular, it was shown that the Mn(V)-oxo porphyrin efficiently reacted with weak hydrogen atom donors via a hydride transfer reaction [46]. In addition, studies of the analogous manganese(V)-oxo corrole and corrolazine complexes have been reported and found to be efficient oxidants of substrate hydroxylation reactions [47–52]. Full understanding of the reaction mechanism of hydride transfer from substrates to metal-oxo oxidants is lacking. For instance, recent studies of 10-methyl-9,10-dihydroacridine ($AcrH_2$) hydroxylation by Mn(V)-oxo complexes [44] seemed to indicate a proton-coupled electron-transfer followed by a fast electron transfer mechanism. In particular, the studies implicated that the second electron transfer was separated from the proton and first electron transfer processes. However, it was not clear from the studies whether the first and rate determining step is a hydrogen atom transfer or a PCET reaction. In order to resolve the reaction mechanism of substrate oxidation by Mn(V)-oxo porphyrin complexes, we have performed a density functional theory (DFT) study, which we present in this work. In addition, we investigated the substrate activation mechanisms by the Mn(IV)-oxo analogue and compare its mechanism and kinetics with those calculated for the Mn(V)-oxo complex. Scheme 2 shows drawings of the oxidants and substrate studied in this work. To validate our findings, we did a series of benchmark studies on the reactant complexes and compared our results with available spectroscopic data on Mn^V=O(TDCPP) with TDCPP = *meso*-tetrakis(2,6-dichlorophenyl)-porphyrin.

Methods

All calculations presented in this work were obtained with density functional theory and employed methods and techniques as reported previously [53]. All geometries described here are the result of a full geometry optimization (without constraints) in *Jaguar* 7.6 [54] followed by an analytical frequency calculation that characterized the stationary points as a local minimum (with real frequencies only) or first order saddle points (transition states) with one imaginary frequency for the correct mode. These calculations use a double-ζ quality LACVP basis set on Mn in combination with 6-31G on all other atoms: basis set B1 [55]. Subsequent single point calculations were done with a triple-ζ quality LACV3P + basis set on Mn and 6-311+G* on the rest of the atoms to improve the energetics: basis set B2. Free energies reported in this work use basis set B2 energies, and basis set B1 calculated zero-point energy (ZPE), and thermal and entropic corrections.

We studied two different manganese-oxo models with chloride axial ligand and either porphyrin (Por) or *meso*-tetrakis(2,6-dichlorophenyl)porphyrin (TDCPP) as equatorial ligand (Scheme 2). The overall charge of the $[Mn^V$=O(Por)Cl] and $[Mn^V$=O(TDCPP)Cl] systems is neutral and they contain close lying singlet and triplet spin state surfaces. The substrate hydroxylation mechanism of 10-methyl-9,10-dihydroacridine ($AcrH_2$) by $[Mn^V$=O(Por)Cl] and its one-electron reduced form, that is $[Mn^{IV}$=O(Por)Cl]$^-$, was investigated and compared to experimental data [46].

It is known from the literature that manganese-based porphyrin complexes are notoriously difficult to describe with DFT methods [56,57]; therefore, we did an extensive set of test calculations with a range of different density functionals. Initially, we did a full geometry optimization of ^{1,3,5}[Mn=O(Por)Cl]^0 using B3LYP [58,59], BP86 [60,61], PBEO [62], PW91B95 [63], and M06 [64] density functional methods. These studies showed that there is some fluctuation in spin state ordering depending on the chosen density functional. To find out whether the spin state ordering is due to differences in ionization potential of the porphyrin ring or whether it is related to the Mn atom, we ran a further series of calculations where we calculated the ionization potential of an isolated porphyrin group ($PorH_2$) and the electron affinity of the bare $[Mn^V$=O]$^{3+}$ group using the B3LYP, BP86, PBEO and PW91B95 methods in combination with a 6-311+G* basis set (LANL2DZ on Mn) in *Gaussian*-03

[65]. To make sure that the choice of the density functional does not affect the conclusions derived from the studies, we ran the subsequent hydroxylation mechanism of $AcrH_2$ by ^{1,3}[Mn=O(Por)Cl] using three different DFT methods, namely B3LYP, BP86 and PBEO. As will be seen later, although some fluctuations are observed between the different density functional methods, the general trends are reproduced well with all methods.

A final set of benchmark studies included calculations of the infrared (IR) and Raman vibrational spectra of ^{3}[Mn^{V}=O(TDCPP)L]$^{+/0}$, L = nothing or Cl^{-}, and its ^{18}O substituted spectrum. Frequencies were scaled with the correction factor of 0.9614 of Scott and Radom [66] and compared to the experimentally reported spectrum from the literature [22].

Results and discussion

Oxo-manganese porphyrin complexes, similar to iron based Cpd I of P450 have many close lying electronic states [67]. Previous studies showed that the reactivity of oxo-manganese porphyrins is dependent on the low-spin/high-spin energy gap [68,69]; therefore, we will start this paper with a detailed description of the electronic configuration and the possible low-lying electronic states. Fig. 1 displays the high-lying occupied and low-lying virtual orbitals of ^{1}[Mn^{V}=O(Por)Cl]^{0}. These orbitals are determined by the metal 3d atomic orbitals that split into the usual $t_{2g} - e_g$ splitting of which the former ones split further into a one-below-two set of orbitals. The lowest one of those is the nonbonding δ_{x2-y2} orbital in the plane of the porphyrin while a pair of antibonding π^* Mn—O orbitals (π^*_{xz}) and (π^*_{yz}) are somewhat higher in energy. Two virtual orbitals represent the two σ^* antibonding orbitals for the Cl—Mn—O bond (σ^*_{z2}) and for the interactions of the metal with the porphyrin nitrogen atoms (σ^*_{xy}). In addition to these five orbitals, similar to [Fe^{IV}=O(Por$^{+\bullet}$)SH] there is also a high-lying porphyrin based orbital that in D_{4h} symmetry has the label a_{2u}. This orbital mixes somewhat with a π-orbital on the axial ligand as also shown here.

The set of orbitals shown in Fig. 1 is occupied by four electrons and consequently there are several possible singlet, triplet and quintet spin state configurations. Thus, the low-spin state with δ^2_{x2-y2} a^2_{2u} configuration represents the closed-shell

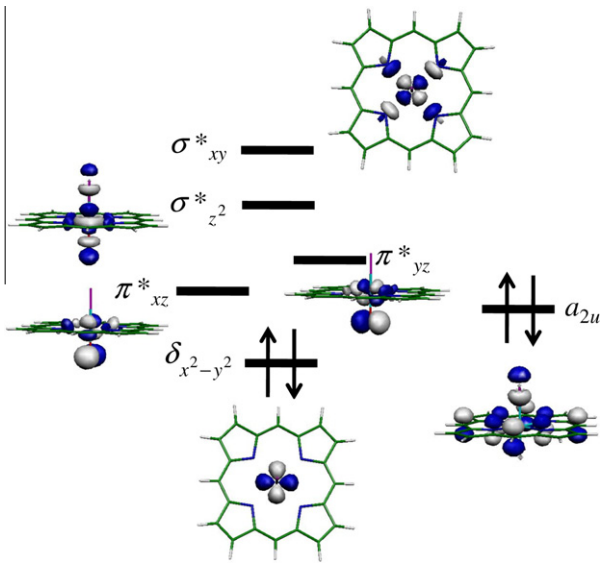

Fig. 1. High-lying occupied and low-lying virtual orbitals of [Mn=O(Por)Cl]^{0}. The orbital occupation is given for ^{1}[Mn^{V}=O(Por)Cl].

^{1}[Mn^{V}=O(Por)Cl]^{0} state. In principle, there are two types of triplet spin states with either a ^{3}[Mn^{V}=O(Por)Cl]^{0} configuration and δ^1_{x2-y2} π^{*1}_{xz} a^2_{2u} occupation or a ^{3}[Mn^{IV}=O(Por$^{+\bullet}$)Cl]^{0} configuration with δ^2_{x2-y2} π^{*1}_{xz} a^1_{2u} configuration. The latter state has the metal in oxidation state Mn(IV) coupled to a porphyrin cation radical, which resembles the electronic configuration of iron based Cpd I of P450 [70]. In the next section we will describe a series of benchmark calculations on the spin state ordering and relative energies of the various low-lying [Mn^{V}=O(Por)Cl]^{0} versus [Mn^{IV}=O(Por$^{+\bullet}$)Cl]^{0} complexes as calculated with a range of DFT methods.

Cpd I of P450 also has two close-lying spin states (doublet and quartet spin), which give rise to two-state reactivity patterns [70]. It is important to ascertain the low-lying spin state surfaces as a potential two-state-reactivity mechanism may apply for oxo-manganese porphyrins as well. In particular, examples have been seen where one spin state surface gives rise to a rearrangement process and the formation of by-products, while on the other spin state surface it is not possible [71–74].

Benchmark studies on ^{1,3,5}[Mn=O(Por)Cl]^{0}

Before embarking on a detailed mechanistic study of substrate hydroxylation by ^{1,3}[Mn^{V}=O(Por)Cl]^{0} versus ^{2,4}[Mn^{IV}=O(Por)Cl]$^{-}$, we decided to do a series of benchmark calculations using a range of different density functional procedures on the possible configurations of [Mn=O(Por)Cl]^{0}. As described in the previous section, the low-lying molecular orbitals shown in Fig. 1 give rise to electronic states with either [Mn^{V}=O(Por)Cl]^{0} or [Mn^{IV}=O(Por$^{+\bullet}$)Cl]^{0} configuration. Although several computational studies on Manganese containing chemical systems reproduced experimental findings [52,75–79], there are several reported cases where the B3LYP method fails [56]. In order to assign the most appropriate density functional method for the studies presented in this work, we decided to do an extensive set of benchmark calculations on our reactant species and establish its low lying electronic states. Electron paramagnetic resonance (EPR) studies characterized [Mn^{V}=O(TDCPP)] as a diamagnetic low-spin d^2 species [20,80].

Table 1 lists relative energies of ^{1,3,5}[Mn=O(Por)Cl]^{0} in the singlet, triplet and quintet spin states as obtained with five different density functional methods: B3LYP, BP86, PBEO, M06, PW91B95. With most DFT methods studied, the lowest lying singlet spin state is ^{1}[Mn^{V}=O(Por)Cl]^{0} with δ^2_{x2-y2} a^2_{2u} configuration in agreement with experimental EPR data, although several DFT methods give a triplet spin ground state instead (B3LYP, PBEO and PW91B95) at least with basis set B1. Notably, the energy difference between the lowest lying triplet and singlet spin states varies strongly between the various DFT methods. In particular, B3LYP predicts the ^{3}[Mn^{IV}=O(Por$^{+\bullet}$)Cl]^{0} state to be the ground state by 8.8 kcal mol^{-1} over the closed-shell singlet state. Also the PW91B95 method predicts this state to be the ground state, but by a much smaller amount (4.9 kcal mol^{-1}). The results are not surprising since these functionals tend to stabilize open-shell systems over closed-shell configurations [57]. With the PBEO density functional we also find a triplet spin ground state, but with orbital occupation δ^1_{x2-y2} π^{*1}_{xz} a^2_{2u} so that this is the ^{3}[Mn^{V}=O(Por)Cl]^{0} configuration. The energy difference between the ^{3}[Mn^{V}=O(Por)Cl]^{0} at PBEO with the closed-shell singlet state is very small (+1.0 kcal mol^{-1}) and the spin state ordering is reversed when the basis set is improved. Attempts to locate the ^{3}[Mn^{IV}=O(Por$^{+\bullet}$)Cl]^{0} states with BP86 and PBEO failed and converged back to the lower lying ^{3}[Mn^{V}=O(Por)Cl]^{0} state, hence the former is an excited state with these methods. Similarly, attempts to swap orbitals in B3LYP, M06 and PW91B95 to obtain the ^{3}[Mn^{V}=O(Por)Cl]^{0} state failed and converged back to the more stable ^{3}[Mn^{IV}=O(Por$^{+\bullet}$)Cl]^{0} state instead. The lowest lying quintet spin state, in all cases, is high in energy and will not take a role

Table 1
Relative energies of low lying electronic configurations of ^{1,3,5}[Mn=O(Por)Cl]^0 as calculated with five different DFT methods.

Configuration	Orbital occupation	Density functional method[a,b,c]				
		B3LYP	BP86	PBEO	M06	PW91B95
^{1}[Mn^V=O(Por)Cl]^0	δ^2_{x2-y2} a^2_{2u}	0.0 (0.0)	0.0 (0.0)	0.0 (0.0)	0.0	0.0
^{1}[Mn^{IV}=O(Por$^{+\bullet}$)Cl]^0	δ^2_{x2-y2} π^{*1}_{xz} a^1_{2u}	0.4				
^{3}[Mn^{IV}=O(Por$^{+\bullet}$)Cl]^0	δ^2_{x2-y2} π^{*1}_{xz} a^1_{2u}	−8.8 (−3.3)			6.8	−4.9
^{3}[Mn^V=O(Por)Cl]^0	δ^1_{x2-y2} π^{*1}_{xz} a^2_{2u}		2.8 (3.9)	−1.0 (1.4)		
^{5}[Mn^{IV}=O(Por$^{+\bullet}$)Cl]^0	δ^1_{x2-y2} π^{*1}_{xz} π^{*1}_{yz} a^1_{2u}	9.5 (10.5)		7.1 (11.0)	2.3	1.1

[a] Relative energies in kcal mol^{-1}.
[b] All data are the result of a B3LYP/B1 geometry optimization followed by frequency analysis.
[c] Values in parenthesis calculated with basis set B2 others with basis set B1.

of importance, therefore, we will focus in the remainder of this work on the singlet and triplet spin states only.

In order to find out whether the scatter of the data in Table 1 is due to differences in ionization potential of the porphyrin ring or due to differences in description of the manganese atoms, we calculated the ionization potential (IP) of an isolated porphyrin group ($PorH_2$) and the electron affinity (EA) of a bare [Mn^V=O]$^{3+}$ molecule. Thus, the calculated 6-311+G* IP values (ΔE + ZPE) for $PorH_2$ are within 0.42 kcal mol^{-1} for the B3LYP, PBEO and PW91B95 methods, while the BP86 datum is 2.49 kcal mol^{-1} above the B3LYP result. The IP difference, therefore, is not the root cause of the state ordering differences in Table 1. However, when we calculate the EA value of [Mn^V=O]$^{3+}$, B3LYP gives 15.8 and 8.4 kcal mol^{-1} larger values than those found for BP86 and PBEO, respectively. Consequently, the B3LYP method will prefer the manganese in lower oxidation states (Mn^{IV}) as compared to BP86 in agreement with the results described in Table 1.

The data shown in Table 1, give quite a bit of scatter and a range of different electronic ground states. Therefore, the reactivity patterns discussed later in this work was investigated with three different DFT methods, namely B3LYP, BP86 and PBEO, which are the three methods that appear to give the largest variation in spin state splitting, whereby B3LYP gives a ^{3}[Mn^{IV}=O(Por$^{+\bullet}$)Cl]^0 ground state, BP86 has a ^{1}[Mn^V=O(Por)Cl]^0 ground state and with PBEO the ^{3}[Mn^V=O(Por)Cl]^0 state is the lowest in energy. Interestingly, a B3LYP calculation on Mn^V-oxo corrolazine complex without axial ligand or with axial ligand (F^- or CN^-) gives a closed-shell singlet ground state that is well separated from the lowest triplet spin state in agreement with experimental data [48]. The disparity of B3LYP observed here, therefore, seems to be restricted to manganese porphyrin complexes only. Previous studies of the Eisenstein group [68,69] on ^{1,3,5}[Mn^V=O(Por)Cl]^0 predicted relative energies of 0.0, 3.4 and 11.1 kcal mol^{-1} for the singlet, triplet and quintet spin states, respectively using the BP86 density functional method. These results are in excellent agreement to our calculated BP86 results reported in Table 1.

Clearly, the [Mn=O(Por)Cl]^0 system appears in many close lying spin states and environmental perturbations, such as a dielectric constant or hydrogen bonding interactions may disrupt the spin state ordering and relative energies. To find out, whether the spin state ordering varies in a dielectric constant or under the influence of a change in chosen basis set, we did some additional calculations on a selection of structures. Thus improving the basis set from B1 to B2 changes the singlet–triplet energy gap (ΔE_{ST}) with all methods in favor of the closed-shell singlet spin state, although in the case of B3LYP the triplet spin state remains the ground state. In the case of B3LYP the ΔE_{ST} value changes from −8.8 to −3.3 kcal mol^{-1}, while inclusion of zero-point energy on these values makes the singlet spin state the ground state albeit by only 1.5 kcal mol^{-1}. It appears, therefore, that zero-point corrections to the energy and single point calculations with basis set B2 are essential to predict the correct ground state with B3LYP. As such, the reactivity studies with substrates will use these methods only.

Similarly to the B3LYP results, using the PBEO density functional method zero-point corrections and single point energy calculations with basis set B2 change the ordering of the spin states and predicts a closed-shell singlet ground state. Thus, with PBEO the singlet–triplet ordering changes with the larger basis set in favor of the singlet spin state by 1.4 kcal mol^{-1}, while zero-point corrections widen this gap further to 3.5 kcal mol^{-1}. Also with BP86 the ΔE_{ST} gap widens from 2.8 to 3.9 kcal mol^{-1}, which implies that the larger basis set is necessary for all density functional methods to predict the correct spin state ordering of our reactant system. Therefore, in our subsequent studies we will only focus on energies obtained with basis set B2 and include zero-point corrections. Recently, we calculated 1-butene epoxidation by [Fe^{IV}=O(Por$^{+\cdot}$)SH] and did geometry optimizations with UB3LYP/B1 as well as with UB3LYP/B2. These studies gave almost identical energies along the reaction mechanism and minor changes in the geometries, therefore, we will use basis set B1 for geometry optimizations here [81].

To further validate the computational methods and the effect of the axial ligand on the calculations, we calculated the vibrational (IR and Raman) frequencies of the ground state of [Mn^V=O(Por)L]$^{+/0}$ with L = nothing or Cl^- using B3LYP/B1 and compared the obtained results with experimental data [82]. Our DFT calculations using the B3LYP density functional method predict an Mn—O stretch vibration (ν_{MnO}) of 497 cm^{-1} for ^{3}[Mn^{IV}=O(Por$^{+\cdot}$)Cl]^0 and 483 cm^{-1} for ^{3}[Mn^{IV}=O(TDCPP$^{+\bullet}$)Cl]^0, whereby the latter vibration shifts by −22 cm^{-1} upon replacement of ^{16}O by ^{18}O. Thus, the resonance Raman spectrum of [Mn^V=O(TM-2-PyP)] with TM-2-PyP = *meso*-tetrakis(*N*-methyl-2-pyridyl)porphyrin gives a signal at 502 cm^{-1} that down-shifts to 475 cm^{-1} upon replacement of ^{16}O by ^{18}O. These vibrations, therefore, are in good agreement with our calculated ν_{MnO} stretch vibrations and so are the calculated ^{16}O/^{18}O changes. On the other hand, we were unable to irrevocably assign an oxygen sensitive vibration in the 700–800 cm^{-1} range, which contrasts the experimental resonance Raman spectrum that predicted a vibration at 759 cm^{-1} that down-shifts by 35 cm^{-1} upon replacement of ^{16}O by ^{18}O. In that particular vibrational region of our spectra we find several vibrational modes where a Mn—O frequency is mixed in, but it was not clear what band corresponds to this frequency.

In summary, DFT benchmark calculations on [Mn=O(Por)Cl]^0 give mixed results on spin state ordering and relative energies, whereas spectroscopic data is reasonably well reproduced. Generally, energies calculated with basis set B2 and corrected for zero-point energies predict the experimentally assigned ^{1}[Mn^V=O(Por)Cl]^0 state as the molecular ground state. However, due to the sensitivity of the methods to spin state ordering, we decided to continue the remainder of the project using three density functional methods, namely BP86, B3LYP and PBEO that display the largest variety of results.

$AcrH_2$ hydroxylation by ^{1,3}[Mn=O(Por)Cl]^0

Recent studies of Fukuzumi and coworkers [46] showed that manganese(V)-oxo porphyrins react with 10-methyl-9,10-dihydroacridine ($AcrH_2$) via a proton-coupled electron-transfer followed by a fast electron transfer. In order to elucidate the full mechanism of $AcrH_2$ hydroxylation we have performed a DFT study. Computational studies of our group on [Fe^{IV}=O($Por^{+\cdot}$)Cl]^0 versus [Fe^{IV}=O(Por)Cl]$^-$ showed that the former reacts via hydride transfer, while the latter via hydrogen atom transfer [83]. Thus, to establish the differences and comparisons between Fe(IV)-oxo porphyrins and Mn(V/IV)-oxo porphyrin, we have studied the $AcrH_2$ hydroxylation by ^{1,3}[Mn=O(Por)Cl]^0 using the BP86, B3LYP and PBEO density functional methods. The mechanism starts from ^{1,3}[Mn=O(Por)Cl]^0 with a hydrogen atom/hydride abstraction transition state (**TS**$_H$) leading to a manganese-hydroxo porphyrin complex (**I**). A subsequent radical rebound transition state (**TS**$_{reb}$) leads to hydroxylated products (**P**). Fig. 2 displays the free energy landscape of substrate ($AcrH_2$) hydroxylation by ^{1,3}[Mn=O(Por)Cl]^0, whereas Fig. 3 gives optimized geometries of the critical points along the reaction mechanism. The choice of the density functional method does not seem to influence the reaction mechanism dramatically, since BP86, B3LYP and PBEO methods all predict a stepwise mechanism via an intermediate (**I**). Similar to previously studied hydrogen abstraction mechanisms [84], also here the hydroxo group in the intermediate complex rebinds to the radical to form alcohol products (**P**) via a rebound transition state (**TS**$_{reb}$).

At the free energy level at 298 K, the singlet and triplet spin states are separated by 0.8 kcal mol^{-1} (B3LYP) and 0.1 kcal mol^{-1} (BP86), which within the error of the calculations implies a degenerate singlet and triplet spin state. B3LYP predicts ^{1}[Mn^V=O(Por)Cl]^0 and ^{3}[Mn^{IV}=O($Por^{+\bullet}$)Cl]^0 to be efficient oxidants of substrate hydroxylation reactions with low H-abstraction reaction barriers of 6.1 and 3.9 kcal mol^{-1}, respectively, in agreement with experimental studies that showed fast and efficient reactions. The barriers obtained with BP86 and PBEO are substantially higher in energy but the ordering remains the same, however, the PBEO method gives high free energies of activation well above 27 kcal mol^{-1} for the H-atom abstraction step, which implies that ^{1,3}[MnO(Por)Cl]^0 is a sluggish oxidant of substrate hydroxylation reactions. The PBEO results are clearly in disparity with experimental observation, hence are probably wrong, but it is not clear why.

All methods predict ^{3}**I** to be lower in energy than ^{1}**I** by about 15 kcal mol^{-1}, although the relative energy with respect to isolated reactants is approximately 10 kcal mol^{-1} more exothermic using the B3LYP method. In all cases the rebound barrier is the rate determining step in the reaction mechanism with barriers of 17.1 and 17.4 kcal mol^{-1} for BP86 and B3LYP, respectively. The driving force from intermediates to products, however, is slightly endothermic in the BP86 results (by +2.1 kcal mol^{-1}), whereas it is exothermic by 10.2 kcal mol^{-1} for B3LYP. Interestingly, the opposite is observed for the singlet spin transfer from intermediate to products, whereby BP86 is exothermic by 2.3 kcal mol^{-1} and B3LYP is endothermic by 9.7 kcal mol^{-1}.

Optimized geometries of the critical points in Fig. 2 are shown in Fig. 3. There are some obvious differences that reflect the large differences in energies discussed above, but generally the geometries of the intermediate and product complexes are very much alike regardless of the chosen density functional method. All three ^{3}**TS**$_H$ barriers are late with longer C—H than O—H bond lengths. Of these three geometries, the one observed for BP86 is the closest to symmetrical with r_{CH} = 1.330 and r_{OH} = 1.254 Å, while substantially different values of r_{CH} = 1.485 and r_{OH} = 1.119 Å are found for B3LYP. Because of the fact that the B3LYP transition state is later than the BP86 transition state also the Mn—O and Mn—Cl distances are longer. A comparison of the singlet spin transition states for B3LYP and BP86 gives similar trends.

Let us in the following give a more in-depth analysis of the computational results. Thus, although the reactant state appears in a singlet spin ground state, the intermediate and product complexes by contrast have a triplet spin ground state with the singlet well higher in energy. This spin state ordering agrees with previous H-abstraction studies of manganese-oxo porphyrin complexes [52,69]. In particular, B3LYP gives a singlet–triplet free energy gap for the intermediate complexes of 16.2 kcal mol^{-1}, while 15.8 kcal mol^{-1} is found from the BP86 results. Therefore, the spin-state ordering and singlet–triplet energies of the intermediate and product complexes are the same for BP86, B3LYP and PBEO. It appears, therefore, that the three methods predict the same trends, and the differences in relative free energies in Fig. 2 arise from differences in the description of the reactant state only. Clearly, the failure of the DFT methods to calculate the ^{1}[Mn=O(Por)Cl]^0 reactant properly has to do with the EA of the Mn=O group. Nevertheless, all DFT studies shown here predict that substrate hydroxylation by ^{1}[Mn^V=O(Por)Cl]^0 proceeds with an initial spin

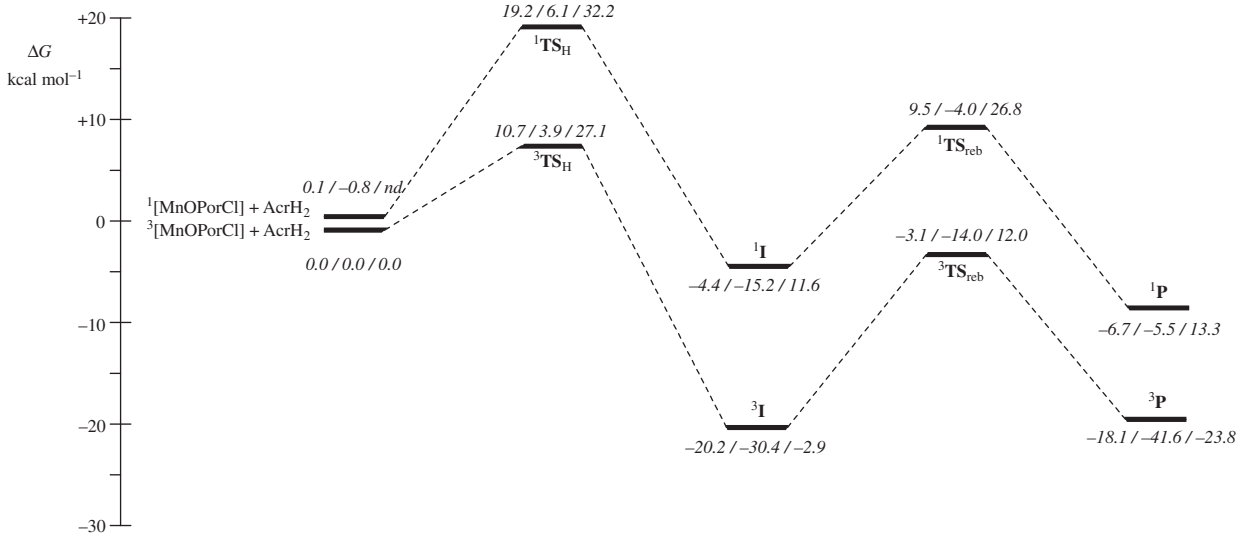

Fig. 2. Free energy landscape of $AcrH_2$ hydroxylation by ^{1,3}[Mn=O(Por)Cl]^0. Energies obtained with basis set B2, while ZPE, thermal and entropic corrections are calculated with basis set B1. The three sets of numbers refer to calculations done using the BP86/B3LYP/PBEO methods.

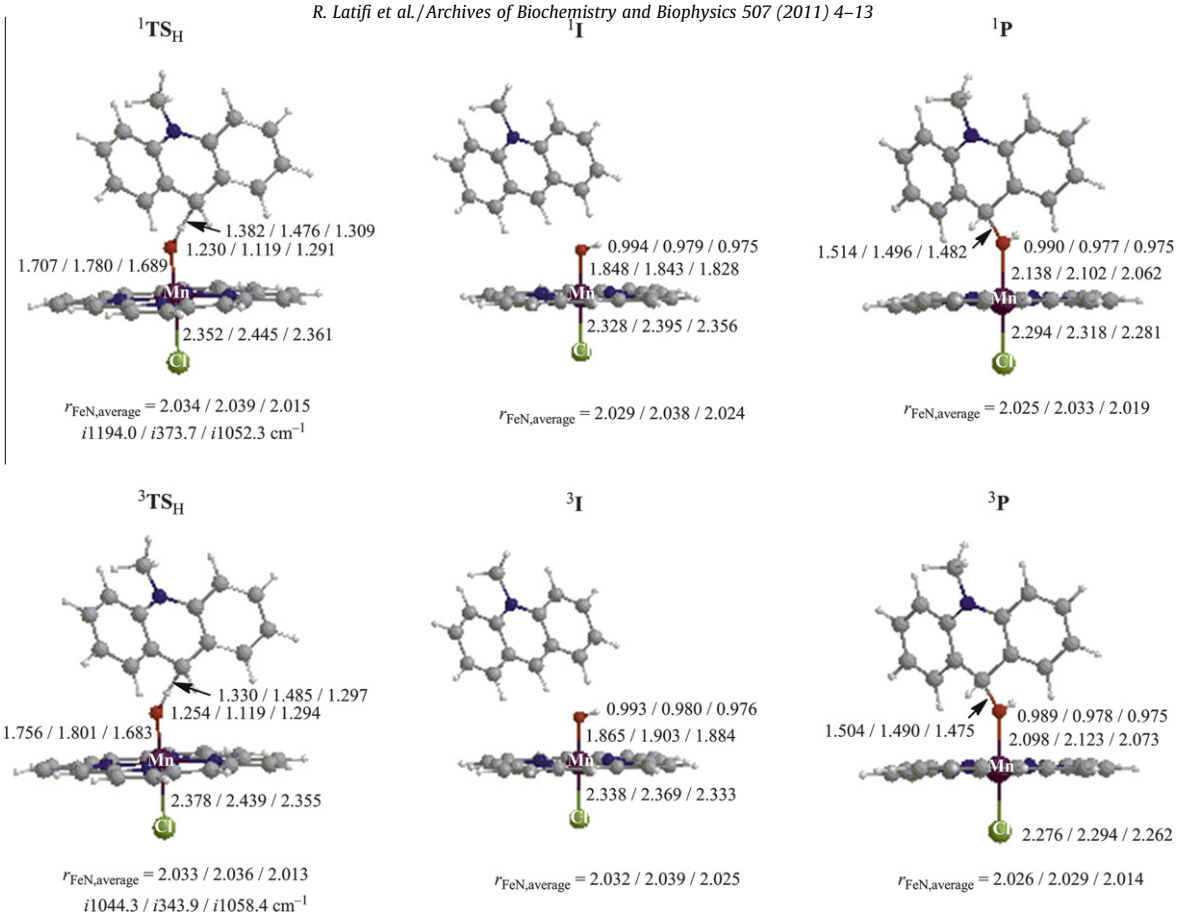

Fig. 3. Optimized geometries of ^{1,3}**TS**$_H$, ^{1,3}**I** and ^{1,3}**P** as calculated with BP86/B3LYP/PBEO methods in combination with basis set B1.

state crossing from singlet to triplet whereby the reaction continues on this surface to give alcohol product complexes. This conclusion is in agreement with previous substrate hydroxylation calculations by manganese-oxo complexes [68,69]. The alternative singlet spin state mechanism leading to products is high in energy due to the lack of available orbitals to accept extra electrons (see below).

To highlight the differences between the mechanisms obtained using B3LYP, BP86 and PBEO, we give the group spin densities of ^{1,3}**TS**$_H$ and ^{1,3}**I** in Tables 2 and 3. The B3LYP and PBEO obtained group spin densities are very much alike and refer to the same electronic situation. Thus, ^{3}**I**(B3LYP) refers to a ^{3}[Mn^{III}(OH)(Por)Cl]—AcrH$^+$ complex with two unpaired electrons on the metal in π^*_{xz} and π^*_{yz} orbitals, i.e. δ^2_{x2-y2} π^{*1}_{xz} π^{*1}_{yz} a^2_{2u} ϕ_{AcrH^0}. This state is the result of a hydride transfer from the substrate to the manganese-oxo center. Although one would expect the group spin densities of the transition states to be midway between the reactant and intermediate configuration this is not the case here. Thus, the corresponding ^{3}**TS**$_H$ structures give approximately two unpaired electrons on the manganese atom indicating single occupation of the π^*_{xz} and π^*_{yz} molecular orbitals and the metal in oxidation state Mn^{III}. In addition, the transition states contain a significant amount of radical character (ρ_{AcrH} = –0.32) on the AcrH restgroup, therefore, the hydride transfer that takes place from reactants to

Table 2
Group spin densities of ^{1,3}**TS**$_H$ as calculated with three different DFT methods and basis set B2.

Method	^{3}**TS**$_H$					^{1}**TS**$_H$				
	ρ_{Mn}	ρ_O	ρ_{Por}	ρ_{Cl}	ρ_{AcrH2}	ρ_{Mn}	ρ_O	ρ_{Por}	ρ_{Cl}	ρ_{AcrH2}
BP86	2.65	0.12	−0.16	0.02	−0.63	0.64	−0.06	−0.05	0.00	−0.53
B3LYP	1.87	0.01	0.36	0.08	−0.32	1.91	−0.06	−0.94	−0.10	−0.81
PBEO	2.96	0.06	−0.26	−0.03	−0.73	2.00	−0.01	−1.05	−0.10	−0.84

Table 3
Group spin densities of ^{1,3}**I** as calculated with three different DFT methods and basis set B2.

Method	^{3}**I**					^{1}**I**				
	ρ_{Mn}	ρ_O	ρ_{Por}	ρ_{Cl}	ρ_{AcrH2}	ρ_{Mn}	ρ_O	ρ_{Por}	ρ_{Cl}	ρ_{AcrH2}
BP86	2.47	0.10	−0.13	0.08	−0.53	0.57	−0.04	−0.03	0.03	−0.52
B3LYP	2.01	0.03	−0.09	0.04	0.01	2.02	0.06	−1.06	−0.05	−0.97
PBEO	2.06	0.03	−0.12	0.03	0.01	2.07	0.05	−1.10	−0.05	−0.98

intermediates formally is a sequential hydrogen atom abstraction followed by electron transfer. Recent studies on $AcrH_2$ hydroxylation by $[Fe^{IV}{=}O(Por^{+\bullet})Cl]^0$ also gave a H-atom abstraction transition state that is followed by a fast electron transfer en route to the intermediate complex to give an overall hydride transfer reaction [83].

In the singlet spin state the situation is quite different using the B3LYP method, whereby a $^1[Mn^{III}(OH)(Por^{+\bullet})Cl]{-}AcrH^{\cdot}$ intermediate (^{1}**I**) is formed with configuration $\delta^2_{x2-y2}\ \pi^{*1}_{xz}\ \pi^{*1}_{yz}\ a^1_{2u}\ \phi_{AcrH}{}^1$, i.e. a hydrogen atom abstraction has occurred rather than a hydride transfer. Formation of this intermediate from the $^1[Mn^{V}{=}O(Por)Cl]^0$ reactant, however, would require a double electron transfer, e.g. from ϕ_{AcrH} to π^* and from a_{2u} to π^*. More likely, this intermediate originates from the $^1[Mn^{IV}{=}O(Por^{+\bullet})Cl]^0$ reactant state by transfer of a single electron from the substrate into the π^*_{yz} molecular orbital.

The electronic states and mechanisms calculated are completely different for BP86 as compared to B3LYP. Thus, starting from $^{1,3}[Mn^{V}{=}O(Por)Cl]^0$ reactants, a hydrogen atom abstraction leads to $^{1,3}[Mn^{IV}{=}O(Por)Cl]{-}AcrH^{\cdot}$ intermediates (^{1,3}**I′**) with orbital occupation $\delta^1_{x2-y2}\ \pi^{*1}_{xz}\ \pi^{*1}_{yz}\ \phi_{AcrH}{}^1$ in the triplet spin state and $\delta^2_{x2-y2}\ \pi^{*1}_{xz}\ \phi_{AcrH}{}^1$ in the singlet spin state.

Based on the electronic spin densities and orbital occupations, we have assigned the electron transfer processes from reactants to intermediates for the various reactant states and the results are summarized in Scheme 3 for completeness. Our three DFT methods give reactant states with configuration $^{1,3}[Mn^{V}{=}O(Por)Cl]^0$ or $^{1,3}[Mn^{IV}{=}O(Por^{+\bullet})Cl]^0$ as described in the previous section. Also the intermediate complexes give a range of possible spin states with different electronic configurations ^{1,3}**I** and ^{1,3}**I′**.

The electronic configuration of ^{1}**I** as calculated with B3LYP, however, is two electrons different from $^1[Mn^{V}{=}O(Por)Cl]^0$, hence would require a double electron transfer, i.e. from the substrate to π^* and an excitation from a_{2u} to π^*. More likely, therefore, is that ^{1}**I** originates from the $^1[Mn^{IV}{=}O(Por^{+\bullet})Cl]^0$ state with $\delta^2_{x2-y2}\ \pi^{*1}_{xz}\ a^1_{2u}$ occupation. The alternative hydrogen atom transfer that gives ^{1}**I′** instead with orbital occupation $\delta^2_{x2-y2}\ \pi^{*1}_{xz}\ a^2_{2u}\ \phi_{AcrH}{}^1$, i.e. $[Mn^{IV}(OH)(Por)Cl]{-}AcrH^{\cdot}$ was also tested but the wave function converged to the lower lying ^{1}**I** solution instead. Therefore, at the B3LYP level ^{1}**I′** is an excited state in favor of ^{1}**I**. DFT calculations on the reactivity of oxo-iron(IV) porphyrin mimics of cytochrome P450, by contrast, usually give $[Fe^{IV}(OH)(Por)L]{-}Sub^{\cdot}$ intermediates in the gas-phase with the $[Fe^{III}(OH)(Por^{+}{\cdot})L]{-}Sub^{\cdot}$ solution at least 4 kcal mol^{-1} higher in energy [85,86]. The manganese porphyrins, therefore, keep the metal in a lower oxidation state during the reaction mechanism.

In the triplet spin state the picture is totally different. Thus, the group spin densities for ^{3}**I** shown in Table 2 indicate $\delta^2_{x2-y2}\ \pi^{*1}_{xz}\ \pi^{*1}_{yz}\ a^2_{2u}\ \phi_{AcrH}{}^0$ configuration, i.e. $Mn^{III}(OH)(Por)Cl{-}AcrH^{-}$. This configuration is the result of a formal hydride transfer in the first step of the reaction mechanism rather than a hydrogen atom transfer on the singlet spin state surface. Thus, fundamentally different reaction mechanisms are obtained on the singlet and triplet spin state surfaces for $^{1,3}[Mn{=}O(Por)Cl]^0$ with $AcrH_2$, whereby the singlet spin state surface gives hydrogen atom transfer, while the triplet spin state surface proceeds via a hydride transfer instead.

Note that in the transition state there is significant radical character on the substrate (ϕ_{AcrH} = –0.32), which implies that the hydride transfer is essentially an initial hydrogen atom transfer, followed by an electron transfer after the transition state. This has been observed before for $AcrH_2$ hydroxylation by $[Fe^{IV}{=}O(Por^{+\bullet})Cl]^0$ [83]. Moreover, experimental studies [46] assigned a PCET mechanism for $AcrH_2$ hydroxylation by Mn(V)-oxo complexes, whereby the second electron transfer is separated from the proton and first electron transfer processes in agreement with what is found here for B3LYP and PBEO. In agreement with the studies of Eisenstein and coworkers no barrier for either hydrogen atom transfer or hydride transfer is found starting from the $^1[Mn^{V}{=}O(Por)Cl]^0$ reactant using the BP86 method [68,69].

$AcrH_2$ hydroxylation by $^{2,4}[Mn{=}O(Por)Cl]^-$

Subsequently, we took the one-electron reduced form of $[Mn^{V}{=}O(Por)Cl]^0$, namely $[Mn^{IV}{=}O(Por)Cl]^-$ and also studied its mechanism of $AcrH_2$ hydroxylation using B3LYP, and the results are shown in Fig. 4.

Thus, one-electron reduction of $^1[Mn^{V}{=}O(Por)Cl]$ gives a doublet spin ground state with electronic configuration $\delta^2_{x2-y2}\ \pi^{*1}_{xz}\ a^2_{2u}$, which is well lower in energy than the quartet spin state with $\delta^1_{x2-y2}\ \pi^{*1}_{xz}\ \pi^{*1}_{yz}\ a^2_{2u}$ configuration by ΔG = 11.8 kcal mol^{-1}, i.e. both doublet and quartet spin states correspond to an $[Mn^{IV}{=}O(Por)Cl]^-$ configuration. Interestingly, a B3LYP calculation for the reduced species does not give evidence of low-lying $[Mn^{III}{=}O(Por^{+\bullet})Cl]$ electronic states, which implies that it is a high lying state that is not accessible. As such, problems in electronic description as a result of changing the DFT method should be considerably less likely here. On both spin state surfaces a hydrogen atom abstraction leads to an intermediate (^{4,2}**I**) with configuration $\delta^2_{x2-y2}\ \pi^{*1}_{xz}\ \pi^{*1}_{yz}\ a^2_{2u}\ \phi_{AcrH}{}^1$, i.e. $[Mn^{III}(OH)(Por)Cl]{-}AcrH^{\cdot}$, whereby the spin on the substrate is either ferromagnetically or antiferromagnetically coupled to the unpaired electrons on the metal in the quartet and doublet spin states. A large rebound barrier leads to product

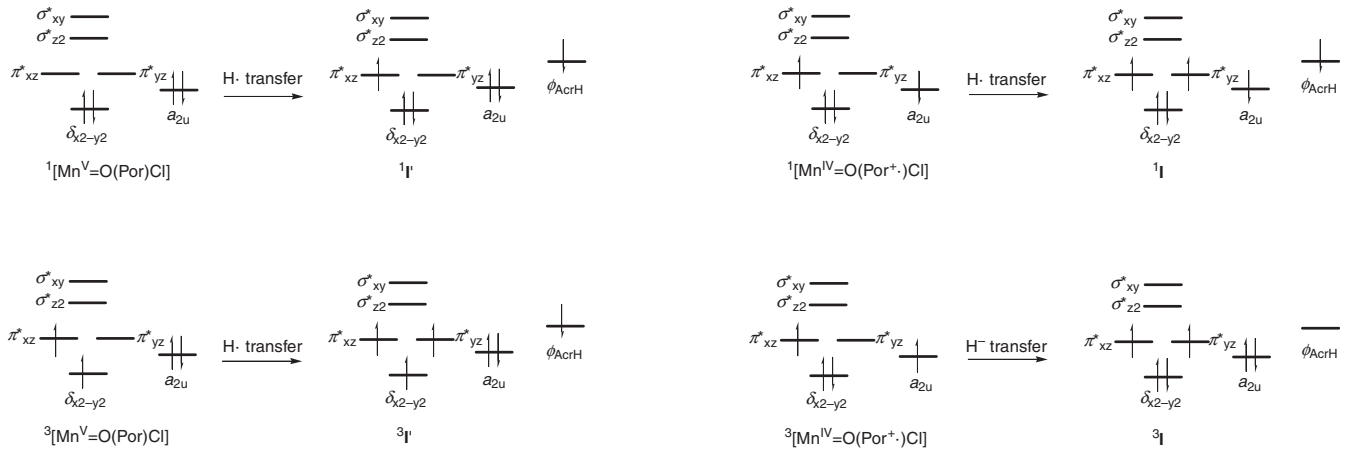

Scheme 3. Electron transfer processes from various reactant states to intermediates.

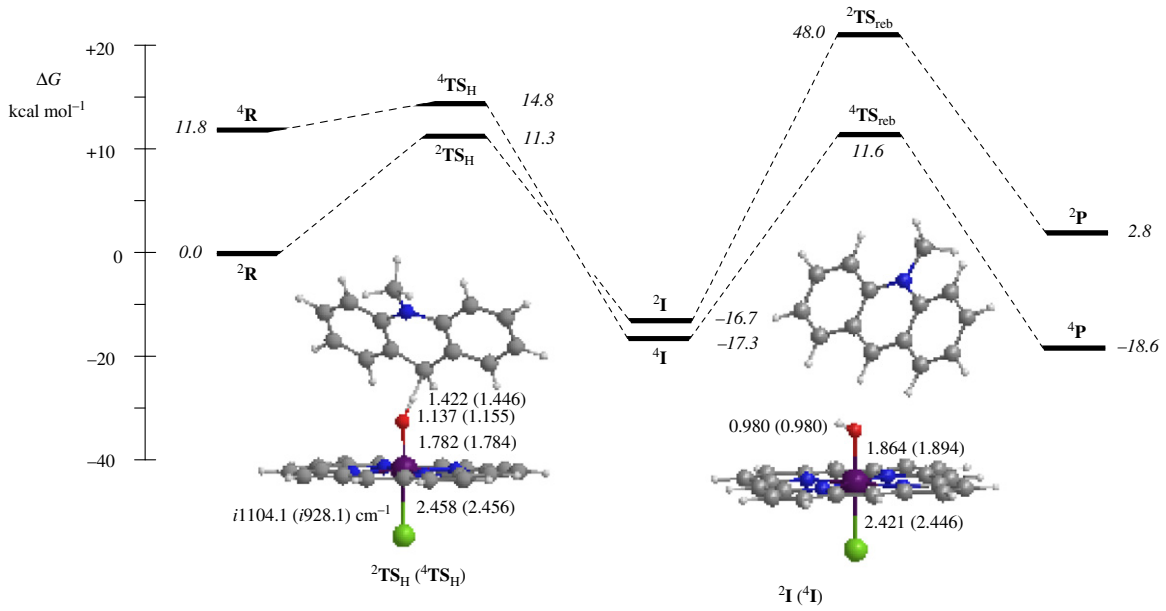

Fig. 4. Potential energy landscape of $AcrH_2$ hydroxylation by $^{2,4}[Mn^{IV}{=}O(Por)Cl]^-$ (^{2,4}**R**) with free energies in kcal mol^{-1}. Values obtained with basis set B2 and contain zero-point, thermal and entropic corrections with basis set B1.

complexes in a slightly endothermic reaction on the quartet spin state surface and an exothermic reaction on the doublet spin state surface. Clearly, a spin state crossing from the doublet to the quartet spin state surface is necessary in or after the intermediate complex to proceed to form alcohol products. As follows from Fig. 4 the rate determining step in the reaction mechanism is the radical rebound barrier rather than the initial hydrogen atom abstraction. This contrasts the reactivity pattern of the $[Mn^{V}{=}O(Por)Cl]^0$ species above, where the rate determining step is via $\mathbf{TS}_H$.

The barrier height calculated with B3LYP is substantially higher for $[Mn^{IV}=O(Por)Cl]^-$ as compared to $[Mn^{V}{=}O(Por)Cl]$, see Figs. 2 and 4. This is in agreement with computational studies of $[Fe^{IV}{=}O(Por^{+\bullet})Cl]$ and its one-electron reduced form [83], where also the reduced species is the weaker oxidant of the two. Nevertheless, the hydrogen abstraction barriers for $AcrH_2$ hydroxylation by $[Mn^{IV}{=}O(Por)Cl]^-$ are sufficiently low to enable efficient hydroxylation of weak C—H bonds. Therefore, based on the B3LYP results we predict both $[Mn^{V}{=}O(Por)Cl]$ and $[Mn^{IV}{=}O(Por)Cl]^-$ to be oxidants of $AcrH_2$ although the former will react faster.

Optimized geometries of transition states and intermediates are in line with those described above in Fig. 3. Generally, $^{4,2}\mathbf{TS}_H$ are late with long C—H and short O—H distances in an intermediate complex type configuration. The imaginary frequencies for $^{4,2}\mathbf{TS}_H$ are large (i1104.1 and i928.1 cm^{-1}, respectively for $^{2}\mathbf{TS}_H$ and $^{4}\mathbf{TS}_H$), but the values are typical for hydrogen abstraction transition states.

So what is the origin of the preference of hydrogen atom abstraction versus hydride transfer in substrate hydroxylation reactions and why is $[Mn^{V}{=}O(Por)Cl]$ a better oxidant than $[Mn^{IV}{=}O(Por)Cl]^-$? To address these questions, let us first consider the thermodynamics of the two reaction processes, i.e. hydrogen atom abstraction (Eq. (1)) versus hydride transfer (Eq. (2)).

$$[Mn^{X}{=}O] + SubH \rightarrow [Mn^{X-1}(OH)] + Sub^{\bullet} + \Delta G_{HA} \quad (1)$$

$$[Mn^{X}{=}O] + SubH \rightarrow [Mn^{X-2}(OH)]^- + Sub^{+} + \Delta G_{HT} \quad (2)$$

Thus, in Eqs. (1) and (2), the formal oxidation state of the metal is X and is reduced by one unit in a hydrogen atom abstraction reaction and the reaction free energy is ΔG_{HA}, whereas the formal oxidation state of the metal is reduced by two units in a hydride transfer reaction with overall reaction free energy ΔG_{HT}. Often reaction energy and barrier height are connected to each other [84,87], therefore, these differences in reaction free energy will enable us to predict the regioselectivity of hydrogen atom transfer versus hydride transfer mechanisms. Thus, a favorable hydrogen atom transfer over hydride transfer will obey the thermodynamical rule:

$$\Delta G_{HA} > \Delta G_{HT} \quad (3)$$

Combination of Eqs. (1)–(3) then gives Eq. 4.

$$\Delta G_{HA} - \Delta G_{HT} > \Delta G([Mn^{X-1}(OH)]) + \Delta G(Sub^{\bullet}) - \Delta G([Mn^{X-2}(OH)]^-) - \Delta G(Sub^{+}) \quad (4)$$

The free energy difference between $[Mn^{X-2}(OH)]^-$ and $[Mn^{X-1}(OH)]$, however, is the electron affinity of $[Mn^{X-1}(OH)]$, $\Delta G_{EA,MnX-1(OH)}$, while the free energy difference between $[Sub^+]$ and $[Sub^{\bullet}]$ equals its ionization potential, IE_{Sub}. Consequently, the difference in reaction enthalpy for hydrogen atom abstraction and hydride transfer is equal to the difference between $\Delta G_{EA,MnX-1(OH)}$ and IE_{Sub}, Eq. (5).

$$\Delta G_{HA} - \Delta G_{HT} > IE_{Sub} - \Delta G_{EA,MnX-1(OH)} \quad (5)$$

Therefore, if the ionization potential of the substrate rest-group is larger than the electron affinity of the manganese-hydroxo complex than hydrogen atom transfer is thermodynamically more exothermic than hydride transfer and more likely to happen. To find out the differences in these reaction free energies for the $[Mn^{V}{=}O(Por)Cl]$ versus $[Mn^{IV}{=}O(Por)Cl]^-$ oxidants described above, we calculated the individual hydrogen atom, electron and hydride transfer reaction free energies from isolated species and the results are schematically depicted in Fig. 5. Note that the hydrogen atom and hydride transfer reactions are calculated relative to $H^{\bullet}$ and H^-, respectively, rather than relative to substrate.

Thus, as follows from Fig. 5 the free energy difference between $[Mn^{IV}(OH)(Por)Cl]$ and the sum of $[Mn^{V}{=}O(Por)Cl]$ and a hydrogen atom is 94.4 kcal mol^{-1}, whereas the free energy difference between $[Mn^{III}(OH)(Por)Cl]^-$ and the sum of $[Mn^{V}{=}O(Por)Cl]$ and a hydride is 202.2 kcal mol^{-1} in the gas phase. Since, the reaction exothermicity is larger for the hydride transfer than for the

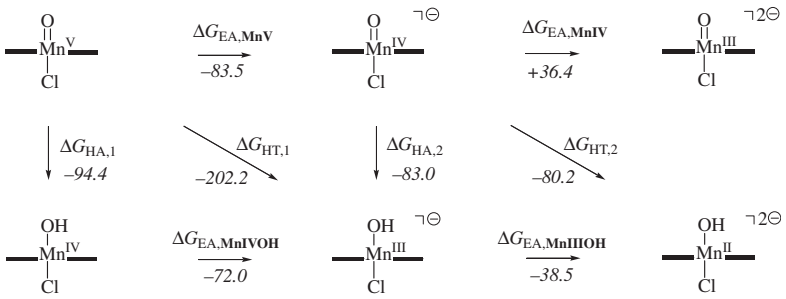

Fig. 5. Relative free energies between manganese-oxo and manganese-hydroxo complexes. Data calculated with B3LYP/B1.

hydrogen atom transfer [Mn^{V}=O(Por)Cl] reacts by preferential hydride transfer from $AcrH_2$. On the other hand, starting from [Mn^{IV}=O(Por)Cl]$^{-}$ the hydrogen atom abstraction energy is more exothermic than the hydride transfer energy, so that it will react via hydrogen atom abstraction rather than hydride transfer. These thermodynamic cycles are in excellent agreement with the reactivity patterns described above in Figs. 2 and 4 and explain the observed reactions. The reason why [Mn^{V}=O(Por)Cl] reacts via hydride transfer, while [Mn^{IV}=O(Por)Cl]$^{-}$ by hydrogen atom abstraction follows from the electron affinities of these oxidants. Thus, the Mn^{V} species has many available low-lying molecular orbitals and accepting two electrons lead to filling of the π^{*}_{xz} and π^{*}_{yz} molecular orbitals with one electron. By contrast, in the Mn^{IV} complex the π^{*}_{xz} orbital is already occupied by one electron, so that a double electron acceptance as happens in a hydride transfer reaction will mean the filling of the π^{*}_{yz} with one electron and addition of a second electron to the π^{*}_{xz} orbital. Alternatively, instead of double occupation of the π^{*}_{xz} orbital an excitation to an empty σ^{*}_{z2} orbital is also possible. Nevertheless, in both cases these electron transfer processes encounter a high energy state and therefore will be thermodynamically costly. Indeed, especially the addition of the second electron starting from the Mn^{IV} complex is energetically unfavorable; hence a hydride transfer is not possible for this complex.

Conclusions

Density functional theory calculations are reported on the reactivities of oxo-manganese porphyrin complexes. It is shown that the several low-lying spin states are involved in the mechanism, but the lowest barriers appear on the triplet spin state surface. Interestingly, the singlet spin surface is a hydrogen atom abstraction, whereas on the triplet spin state a hydride is abstracted, although the hydride transfer reaction is a hydrogen atom abstraction followed by electron transfer. As such, the latter is more exothermic and proceeds with lower barriers, so that a spin-state crossing from singlet to triplet is required for the reaction. Subsequent calculations of $AcrH_2$ hydroxylation by [Mn^{IV}=O(Por)Cl]$^{-}$ show it to be a lesser good oxidant than [Mn^{V}=O(Por)Cl]. Moreover, with [Mn^{IV}=O(Por)Cl]$^{-}$ the rate determining step is the radical rebound rather than the initial hydrogen atom abstraction.

Acknowledgments

The National Service of Computational Chemistry Software (NSCCS) is acknowledged for CPU time provided. S.P.D.V. thanks the Royal Society of Chemistry for an RSC Journal Grant. R.L. and L.T. thank the British Council for an Exchange grant. W.N. acknowledges financial support from the NSF/MEST of Korea through the CRI Program and the WCU Program (R31-2008-000-10010-0).

References

[1] M. Sono, M.P. Roach, E.D. Coulter, J.H. Dawson, Chem. Rev. 96 (1996) 2841–2887.
[2] F.P. Guengerich, Chem. Res. Toxicol. 14 (2001) 611–650.
[3] J.T. Groves, Proc. Natl. Acad. Sci. USA 100 (2003) 3569–3574.
[4] P.R. Ortiz de Montellano (Ed.), Cytochrome P450: Structure, Mechanism and Biochemistry, third ed., Kluwer Academic/Plenum Publishers, New York, 2004.
[5] A.W. Munro, H.M. Girvan, K.J. McLean, Nat. Prod. Rep. 24 (2007) 585–609.
[6] K.M. Kadish, K.M. Smith, R. Guilard (Eds.), The Porphyrin Handbook, Academic Press, San Diego, CA, 2010, p. vol. 5.
[7] J.T. Groves, Models and mechanisms of cytochrome P450 action, in: P.R. Ortiz de Montellano (Ed.), Cytochrome P450: Structure, Mechanism and Biochemistry, third ed., Kluwer Academic/Plenum Publishers, New York, 2005, Chapter 1, pp 1–44.
[8] W. Nam, Acc. Chem. Res. 40 (2007) 522–531.
[9] T. Egawa, H. Shimada, Y. Ishimura, Biochem. Biophys. Res. Commun. 201 (1994) 1464–1469.
[10] D.G. Kellner, S.-C. Hung, K.E. Weiss, S.G. Sligar, J. Biol. Chem. 277 (2002) 9641–9644.
[11] H. Fujii, Coord. Chem. Rev. 226 (2002) 51–60.
[12] D. Dolphin, T.G. Traylor, L.Y. Xie, Acc. Chem. Res. 30 (1997) 251–259.
[13] B. Meunier, Chem. Rev. 92 (1992) 1411–1456.
[14] Y.M. Goh, W. Nam, Inorg. Chem. 38 (1999) 914–920.
[15] T.M. Makris, K. von Koenig, I. Schlichting, S.G. Sligar, J. Inorg. Biochem. 100 (2006) 507–518.
[16] H. Hirao, K.-B. Cho, S. Shaik, J. Biol. Inorg. Chem. 13 (2008) 521–530.
[17] T.A. Jackson, T.C. Brunold, Acc. Chem. Res. 37 (2004) 461–470.
[18] D. Mansuy, Coord. Chem. Rev. 125 (1993) 129–141.
[19] J.T. Groves, J. Lee, S.S. Marla, J. Am. Chem. Soc. 119 (1997) 6269–6273.
[20] N. Jin, J.T. Groves, J. Am. Chem. Soc. 121 (1999) 2923–2924.
[21] W. Nam, I. Kim, M.H. Lim, H.J. Choi, J.S. Lee, H.G. Jang, Chem. Eur. J. 8 (2002) 2067–2071.
[22] W.J. Song, M.S. Seo, S. DeBeer George, T. Ohta, R. Song, M.-J. Kang, T. Tosha, T. Kitagawa, E.I. Solomon, W. Nam, J. Am. Chem. Soc. 129 (2007) 1268–1277.
[23] N. Jin, M. Ibrahim, T.G. Spiro, J.T. Groves, J. Am. Chem. Soc. 129 (2007) 12416–12417.
[24] Y. Shimazaki, T. Nagano, H. Takesue, K. Ichihara, B.-H. Ye, F. Tani, Y. Naruta, Angew. Chem. Int. Ed. 42 (2004) 98–100.
[25] E. Rose, B. Andrioletti, S. Zrig, M. Quelquejeu-Ethève, Chem. Soc. Rev. 34 (2005) 573–583.
[26] S.-E. Park, W.J. Song, Y.O. Ryu, M.H. Lim, R. Song, K.M. Kim, W. Nam, J. Inorg. Biochem. 99 (2005) 424–431.
[27] G. Yin, M. Buchalova, A.M. Danby, C.M. Perkins, D. Kitko, J.D. Carter, W.M. Scheper, D.H. Busch, Inorg. Chem. 45 (2006) 3467–3474.
[28] J.P. Collman, L. Zeng, H.J.H. Wang, A. Lei, J.I. Brauman, Eur. J. Org. Chem. (2006) 2707–2714.
[29] K. Nehru, S.J. Kim, I.Y. Kim, M.S. Seo, Y. Kim, S.-J. Kim, J. Kim, W. Nam, Chem. Commun. (2007) 4623–4625.
[30] J.A.A.W. Elemans, E.J.A. Bijsterveld, A.E. Rowan, R.J.M. Nolte, Eur. J. Org. Chem. (2007) 751–757.
[31] R.L. Shook, A.S. Borovik, Chem. Commun. (2008) 6095–6107.
[32] J.F. Hull, E.L.O. Sauer, C.D. Incarvito, J.W. Faller, G.W. Brudvig, R.H. Crabtree, Inorg. Chem. 48 (2009) 488–495.
[33] Z. Gross, G. Golubkov, L. Simkhovich, Angew. Chem. Int. Ed. 39 (2000) 4045–4047.
[34] H.-Y. Liu, T.-S. Lai, L.-L. Yeung, C.K. Chang, Org. Lett. 5 (2003) 617–620.
[35] H.-Y. Liu, F. Yam, Y.T. Xie, X.Y. Li, C.K. Chang, J. Am. Chem. Soc. 131 (2009) 12890–12891.
[36] R. Zhang, M. Newcomb, J. Am. Chem. Soc. 125 (2003) 12418–12419.
[37] R. Zhang, J.H. Horner, M. Newcomb, J. Am. Chem. Soc. 127 (2005) 6573–6582.
[38] R.L. Shook, A.S. Borovik, Inorg. Chem. 49 (2010) 3646–3660.
[39] T.H. Parsell, M.-Y. Yang, A.S. Borovik, J. Am. Chem. Soc. 131 (2009) 2762–2763.
[40] T.H. Parsell, R.K. Behan, M.T. Green, M.P. Hendrich, A.S. Borovik, J. Am. Chem. Soc. 128 (2006) 8728–8729.

[41] G. Yin, J.M. McCormick, M. Buchalova, A.M. Danby, K. Rodgers, V.W. Day, K. Smith, C.M. Perkins, D. Kitko, J.D. Carter, W.M. Scheper, D.H. Busch, Inorg. Chem. 45 (2006) 8052–8061.
[42] G. Yin, A.M. Danby, D. Kitko, J.D. Carter, W.M. Scheper, D.H. Busch, J. Am. Chem. Soc. 129 (2007) 1512–1513.
[43] G. Yin, A.M. Danby, D. Kitko, J.D. Carter, W.M. Scheper, D.H. Busch, J. Am. Chem. Soc. 130 (2008) 16245–16253.
[44] T. Kurahashi, A. Kikuchi, T. Tosha, Y. Shiro, T. Kitagawa, H. Fujii, Inorg. Chem. 47 (2008) 1674–1686.
[45] J.F. Hull, D. Balcells, E.L.O. Sauer, C. Raynaud, G.W. Brudvig, R.H. Crabtree, O. Eisenstein, J. Am. Chem. Soc. 132 (2010) 7605–7616.
[46] J.Y. Lee, Y.-M. Lee, H. Kotani, W. Nam, S. Fukuzumi, Chem. Commun. (2009) 704–706.
[47] B.S. Mandimutsira, B. Ramdhanie, R.C. Todd, H. Wang, A.A. Zareba, R.S. Czernuszewicz, D.P. Goldberg, J. Am. Chem. Soc. 124 (2002) 15170–15171.
[48] S.H. Wang, B.S. Mandimutsira, R. Todd, B. Ramdhanie, J.P. Fox, D.P. Goldberg, J. Am. Chem. Soc. 126 (2004) 18–19.
[49] D.E. Lansky, B. Mandimutsira, B. Ramdhanie, M. Clausén, J. Penner-Hahn, S.A. Zvyagin, J. Telser, J. Krzystek, R. Zhan, Z. Ou, K.M. Kadish, L. Zakharov, A.L. Rheingold, D.P. Goldberg, Inorg. Chem. 44 (2005) 4485–4498.
[50] G. Golubkov, J. Bendix, H.B. Gray, A. Mahammed, I. Goldberg, A.J. Dibilio, Z. Gross, Angew. Chem. Int. Ed. 40 (2001) 2132–2134.
[51] Z. Gross, G. Golubkov, L. Simkhovich, Angew. Chem. Int. Ed. 39 (2000) 4045–4048.
[52] K.A. Prokop, S.P. de Visser, D.P. Goldberg, Angew. Chem. Int. Ed. 49 (2010) 5091–5095.
[53] S.P. de Visser, J. Am. Chem. Soc. 128 (2006) 15809–15818.
[54] *Jaguar* 7.6, Schrödinger, LLC., New York NY, 2007.
[55] P.J. Hay, W.R. Wadt, J. Chem. Phys. 82 (1985) 270–310.
[56] A. Ghosh, P.R. Taylor, Curr. Opin. Chem. Biol. 7 (2003) 113–124.
[57] W.M.C. Sameera, J.E. McGrady, Dalton Trans. (2008) 6141–6149.
[58] A.D. Becke, J. Chem. Phys. 98 (1993) 5648–5652.
[59] C. Lee, W. Yang, R.G. Parr, Phys. Rev. B 37 (1988) 785–789.
[60] A.D. Becke, Phys. Rev. A 38 (1988) 3098–3100.
[61] J.P. Perdew, Phys. Rev. B 33 (1986) 8822–8824.
[62] J.P. Perdew, K. Burke, M. Ernzerhof, Phys. Rev. Lett. 77 (1996) 3865–3868.
[63] Y. Zhao, D.G. Truhlar, J. Phys. Chem. A 109 (2005) 5656–5667.
[64] Y. Zhao, D.G. Truhlar, J. Phys. Chem. A 110 (2006) 13126–13130.
[65] M.J. Frisch, G.W. Trucks, H.B. Schlegel, G.E. Scuseria, M.A. Robb, J. R. Cheeseman, J.A. Montgomery, Jr., T. Vreven, K.N. Kudin, J.C. Burant, J.M. Millam, S.S. Iyengar, J. Tomasi, V. Barone, B. Mennucci, M. Cossi, G. Scalmani, N. Rega, G.A. Petersson, H. Nakatsuji, M. Hada, M. Ehara, K. Toyota, R. Fukuda, J. Hasegawa, M. Ishida, T. Nakajima, Y. Honda, O. Kitao, N. Nakai, M. Klene, X. Li, J.E. Knox, H.P. Hratchian, J.B. Cross, C. Adamo, J. Jaramillo, R. Gomperts, R.E. Stratmann, O. Yazyev, A.J. Austin, R. Cammi, C. Pomelli, J.W. Ochterski, P.Y. Ayala, K. Morokuma, G.A. Voth, P. Salvador, J.J. Dannenberg, V.G. Zakrzewski, S. Dapprich, A.D. Daniels, M.C. Strain, O. Farkas, D.K. Malick, A.D. Rabuck, K. Raghavachari, J.B. Foresman, J.V. Ortiz, Q. Cui, A.G. Baboul, S. Clifford, J. Cioslowski, B.B. Stefanov, G. Liu, A. Liashenko, P. Piskorz, I. Komaromi, R.L. Martin, D.J. Fox, T. Keith, M.A. Al–Laham, C.Y. Peng, A. Nanayakkara, M. Challacombe, P.M. W. Gill, B. Johnson, W. Chen, M.W. Wong, C. Gonzalez, J.A. Pople, Gaussian 03, Revision C.02, Gaussian, Inc., Wallington, CT, 2004.
[66] A.P. Scott, L. Radom, J. Phys. Chem. 100 (1996) 16502–16513.
[67] S.P. de Visser, S. Shaik, P.K. Sharma, D. Kumar, W. Thiel, J. Am. Chem. Soc. 125 (2003) 15779–15788.
[68] D. Balcells, C. Raynaud, R.H. Crabtree, O. Eisenstein, Inorg. Chem. 47 (2008) 10090–10099.
[69] D. Balcells, C. Raynaud, R.H. Crabtree, O. Eisenstein, Chem. Commun. (2008) 744–746.
[70] S. Shaik, S.P. de Visser, F. Ogliaro, H. Schwarz, D. Schröder, Curr. Opin. Chem. Biol. 6 (2002) 556–567.
[71] S.P. de Visser, F. Ogliaro, S. Shaik, Angew. Chem. Int. Ed. 40 (2001) 2871–2874.
[72] D. Kumar, S.P. de Visser, S. Shaik, J. Am. Chem. Soc. 125 (2003) 13024–13025.
[73] D. Kumar, S.P. de Visser, P.K. Sharma, S. Cohen, S. Shaik, J. Am. Chem. Soc. 126 (2004) 1907–1920.
[74] S.P. de Visser, Chem. Eur. J. 12 (2006) 8168–8177.
[75] P. Banerjee, S. Sproules, T. Weyhermüller, S. DeBeer George, K. Wieghardt, Inorg. Chem. 48 (2009) 5829–5847.
[76] J. Annaraj, J. Cho, Y.-M. Lee, S.Y. Kim, R. Latifi, S.P. de Visser, W. Nam, Angew. Chem. Int. Ed. 48 (2009) 4150–4153.
[77] D. Quiñonero, D.G. Musaev, K. Morokuma, Theochemistry 903 (2009) 115–122.
[78] V. Georgiev, T. Borowski, P.E.M. Siegbahn, J. Biol. Inorg. Chem. 11 (2006) 571–585.
[79] V. Georgiev, T. Borowski, M.R.A. Blomberg, P.E.M. Siegbahn, J. Biol. Inorg. Chem. 13 (2008) 929–940.
[80] N. Jin, J.L. Bourassa, S.C. Tizio, J.T. Groves, Angew. Chem. Int. Ed. 39 (2000) 3849–3851.
[81] D. Kumar, B. Karamzadeh, G.N. Sastry, S.P. de Visser, J. Am. Chem. Soc. 132 (2010) 7656–7667.
[82] R.S. Czernuszewicz, Y.O. Su, M.K. Stern, K.A. Macor, D. Kim, J.T. Groves, T.G. Spiro, J. Am. Chem. Soc. 110 (1988) 4158–4165.
[83] L. Tahsini, M. Bagherzadeh, W. Nam, S.P. de Visser, Inorg. Chem. 48 (2009) 6661–6669.
[84] S.P. de Visser, J. Am. Chem. Soc. 132 (2010) 1087–1097.
[85] D. Kumar, S.P. de Visser, S. Shaik, Chem. Eur. J. 11 (2005) 2825–2835.
[86] S.P. de Visser, L. Tahsini, W. Nam, Chem. Eur. J. 15 (2009) 5577–5587.
[87] S. Shaik, D. Kumar, S.P. de Visser, J. Am. Chem. Soc. 130 (2008) 10128–10140.